Research Article Open Access

Seied Mahdi Pourmortazavi, Mehdi Rahimi-Nasrabadi, Mohammad Reza Ganjali, Meisam Sadeghpour Karimi, Parviz Norouzi, Farnoosh Faridbod

Facile and Effective Synthesis of Praseodymium Tungstate Nanoparticles through an Optimized Procedure and Investigation of Photocatalytic Activity

DOI 10.1515/chem-2017-0014 received July 10, 2016; accepted March 29, 2017.

Abstract: Regarding the importance of nanoparticles in today's world, and in the light of the fact that their preparation can be a rather difficult task, we focused on the applicability of a simplistic direct precipitation approach for the preparation of praseodymium tungstate nanoparticles. To maximize the effectiveness of the method, a Taguchi robust design approach was applied to optimize the reaction in terms of the operating conditions influencing its outcome and the results were monitored by characterization of the Pr₂(WO₄)₃ nanoparticles. Among the four parameters studied we found the dimensions of the produced nanoparticles to be determined by the concentrations of Pr^{3+} and $WO_{_{4}}{}^{3-}$ solutions and the reaction temperature, while the flow rate of adding the cation solutions to the anion solution was found to leave very negligible effects on the product characteristics. To confirm the effect of the optimizations on the outcomes of the reaction, SEM, TEM, EDX, XRD, FT-IR and UV-Vis structural and morphological characterizations of the

*Corresponding author: Seied Mahdi Pourmortazavi: Faculty of Material and Manufacturing Technologies, Malek Ashtar University of Technology, Tehran, Islamic Republic of Iran, E-mail: pourmortazavi@yahoo.com; Mehdi Rahimi-Nasrabadi: Faculty of Pharmacy, Baqiyatallah University of Medical Sciences, Tehran, Islamic Republic of Iran; Department of Chemistry, Imam Hossein University, Tehran, Islamic Republic of Iran, E-mail: rahiminasrabadi@gmail.com

Mohammad Reza Ganjali, Parviz Norouzi, Farnoosh Faridbod: Center of Excellence in Electrochemistry, University of Tehran, Tehran, Islamic Republic of Iran; Biosensor Research Center, Endocrinology & Metabolism Molecular-Cellular Sciences Institute, Tehran University of Medical Sciences, Tehran, Islamic Republic of Iran Meisam Sadeghpour Karimi: Faculty of Chemistry and Chemical Engineering, Malek Ashtar University of Technology, Tehran, Islamic Republic of Iran

products were performed, the results of which were in agreement with those statistically predicted in the optimization procedure. Furthermore, as-synthesized praseodymium tungstate nanoparticles under ultraviolet light exhibited an efficient photocatalyst property in the photocatalytic degradation of methylene blue.

Keywords: Nanoparticles; Praseodymium; Tungstate; Process optimization; Photocatalyst

1 Introduction

Benefiting from the attractive properties of nanotechnology (e.g. quantum size effects [1-2] and above normal luminescence phenomenon [3]), which can be achieved through the application of nanosized particles has been a major area of focus in the past decades. Molybdates and tungstates of trivalent metals are among the materials with exciting fluorescent, laser, piezoelectric, ferroelectric and ferroelastic properties [4-6]. These compounds can have a variety of structures and many of them display negative thermal expansion.

Recent research works have paid specific attention to long-life, highly efficient luminescent materials with high quantum yields and emission intensities and their applications in solid-state lasers, amplifying devices and materials, phosphors for color televisions, fluorescent tubes, medical images and luminescent paints [7,8]. Tungstate salts of rare earth cations have specifically been attractive due to the advantages they offer in laser technologies [9].

Among the different rare earth ions, Pr^{3+} offers distinctive properties, due to the possibility of simultaneous blue $(^{3}P_{0} \rightarrow ^{3}H_{4})$, green $(^{3}P_{1} \rightarrow ^{3}H_{5})$, red $(^{3}P_{0} \rightarrow ^{3}F_{2})$, and deep red $(^{3}P_{0} \rightarrow ^{3}F_{4})$ emissions that are possible based

on its electronic configuration [10]. The spectroscopic properties of the ion in several matrices including glasses [9], polycrystals [10], powders [11], and gels [12] have been investigated. Further, the compounds resulting from the reactions between Pr³⁺ with different anions like tungstate [13], vanadate [14], molybdenate [15], titanate [16] which are donors in energy transfer processes, create the promise of advances in the area of visible solid state devices. The nature of the emissions by Pr³⁺ ions is greatly dependent on the host matrix, e.g. perovskite oxides like CaTiO₂:Pr³⁺ or SrTiO_a:Pr³⁺ emit red light with a maximum located at about 618 nm [16].

Removing organic and inorganic pollutants from wastewater under UV or near-UV light in the presence of photocatalyst is a facile and cheap method [17,18], while most of the pollutants could be degraded or mineralized under photocatalytic degradation conditions. During photocatalytic degradation, as a particular photochemical oxidative process, the surface of semiconductor is activated by UV-light in order to generate free radicals from the adsorbed OH species, while the radicals are responsible for degradation of the contaminants. The photocatalytic action is carried out at the surface of the photocatalyst particles. Thus, reducing the mean size of particles in the particulate systems is predictable to improve the interfacial charge transferring degree. The specific surface area of the materials rises due to the particle size reduction and consequently the quantity of the active sites at their surface is enhanced and therefore more absorbed molecules will be able to react with the photo-generated charge carriers to yield hydroxyl and superoxide radicals [17].

This study mainly focuses on the development of an effective route for the preparation of Pr₂(WO₄)₂ through the optimization of the so-called direct precipitation reaction (DPR), with the qualities of being capable of producing praseodymium tungstate nanoparticles with acceptable composition and morphological properties in the absence of surface active compounds, templates or catalytic mechanism. This is a new area of endeavor, based on the results of our literature survey [19-22] on the methods used for the synthesis of Pr₂(WO₄), micro and nanoparticles. Furthermore, methyl blue (MB) degradation was used as a probe reaction to test the as-synthesized Pr₂(WO₄)₂ nanoparticles photoactivity. To the best of our knowledge, synthesis of praseodymium tungstate nano-structures has not been reported previously.

2 Experimental

2.1 The direct precipitation reaction

All salts were purchased from Merck and were used as received. The method for the preparation of the Pr₂(WO₄)₂ particles included the addition of different concentrations of Pr³⁺, at different flow rates, to tungstate solutions. Vigorous stirring regimes were applied and the reaction temperature was also altered at some levels. The final product was filtered and cleaned to remove contaminating residues by distilled water followed by ethanol, before drying at 70°C for 2 hours. The optimization procedure included studying the effect of operating conditions including the concentrations of the cation and anion solutions, their addition flow rates as well as the reaction temperature through an experimental design approach. The mentioned parameters (i.e. Pr³⁺ and tungstate ion concentrations, praseodymium solution flow rate, and reactor temperature) were studied at three different levels according to Table 1.

2.2 Characterization of the produced particles

The characterization of the sample was performed to evaluate its morphology, dimensions, chemical composition and purity. A Philips XL30 series scanning electron microscopy (SEM) instrument and a gold foil for loading the sample were used for acquiring the SEM images and energy-dispersive analysis by X-rays (EDX). For the preparation of the Au foils a SCD005 sputter coater (BAL-TEC Switzerland) was used. X-ray diffraction (XRD) tests were conducted using a Rigaku D/max 2500V diffractometer with a graphite monochromator and a Cu target. The infrared studies were conducted using a Bruck Equinox 55 device and the KBr pellet technique.

For acquiring the UV-Vis spectra the produced particles were dispersed in distilled water and the mixture was analyzed by a Perkin Elemer, Lambda 35 instrument in the wavelength range of 200-700 nm. Transmission electron microscopic images were recorded with a Ziess- EM900 TEM, on samples coated on a Cu grid coated with a layer of carbon. The UV-Vis diffuse reflectance spectra were recorded at room temperature using Avantes Spectrometer Avaspec-2048-TEC.

Table 1: OA₂ (3⁴) matrix applied for optimization of synthesis procedure.

Experiment Number	Pr ³⁺ Concentration (M)	WO ₄ ²⁻ Concentration (M)	Pr ³⁺ Feed flow rate (ml/min)	Temperature (°C)	Average Diameter of Pr ₂ (WO ₄) ₃ particles (nm)		
1	0.005	0.005	2.5	0	63		
2	0.005	0.01	10.0	30	57		
3	0.005	0.1	40.0	60	51		
4	0.01	0.005	10.0	60	57		
5	0.01	0.01	40.0	0	59		
6	0.01	0.1	2.5	30	56		
7	0.1	0.005	40.0	30	63		
8	0.1	0.01	2.5	60	55		
9	0.1	0.1	10.0	0	59		

2.3 Photocatalyst property evaluation

The photocatalytic activity evaluation of as-synthesized praseodymium tungstate nanoparticles was carried out by following the methylene blue (MB) degradation (as an organic pollutant) under UV irradiation using 500 mL aqueous solution of 25 mg/L MB, while praseodymium tungstate nanoparticles (0.1 g/L) were dispersed in the solution. To reach adsorption equilibrium, the studied solution was aerated for 30 minutes via a quartz double pipe air lift photocatalytic reactor equipped with magnetic stirring. A high pressure Hg lamp (250W and λ <280 nm) stayed on the inside of interior pipe of the reactor was utilized for UV irradiation. At various time intervals of irradiation (0, 10, 20, 30, 40, 50, and 60 minutes), the concentration of MB was monitored by analyzing on a UV-Vis spectrophotometer. The photocatalytic activity of the samples was studied at room temperature. Also, the photocatalytic activity of prepared nanoparticles at optimal conditions was compared with the Degussa P25 TiO, under the similar conditions.

3 Results and discussion

It is clear that the dimensions and morphology of particles produced through the precipitation reaction are determined by experimental factors [23], and hence an orthogonal array design (OAD) was used to optimize the experimental conditions based on the evaluation of a rather limited number of experimental results. This optimization technique is a fractional factorial design,

which applies an orthogonal array for attributing the prominent process factors among a set of experimental combinations [24-26], with the aim of characterizing a complicated process with the minimum number of experiments through the specialized design of experiments and statistical approaches to the interpretation of the data [27]. The results of the OAD experiments were further assessed through analysis of variance to explain and confirm significance of tested experimental factors [28]. The application of precipitation reactions for the preparation of insoluble inorganic salts is a potentially useful and conventional technique [29-31] which suffers the disadvantage of lacking control over the properties of the product which gains prominence in the case of nanomaterials which require a high level of control for fine tuning the size and shape of the product. This naturally requires very extensive and thorough knowledge of the interactions between the reagents. However, approaches like the Taguchi robust design can be used to do this more easily. In this work we considered the concentrations of Pr³⁺ and WO₄²⁻ ions, as well as their addition flow rate or F_a (the flow rate at which the Pr³⁺solution was added to the WO₂ solution), and the reactor temperature, at three levels according to the requirements of the Taguchi design, and the results are reported in Table 1.

Several samples were prepared according to the conditions mentioned in this table and they were characterized through the SEM technique, and the resulting SEM images are shown in Figure 1. These results indicate that the dimensions of the produced nanoparticles vary greatly upon altering the operating conditions. To understand the influences of altering

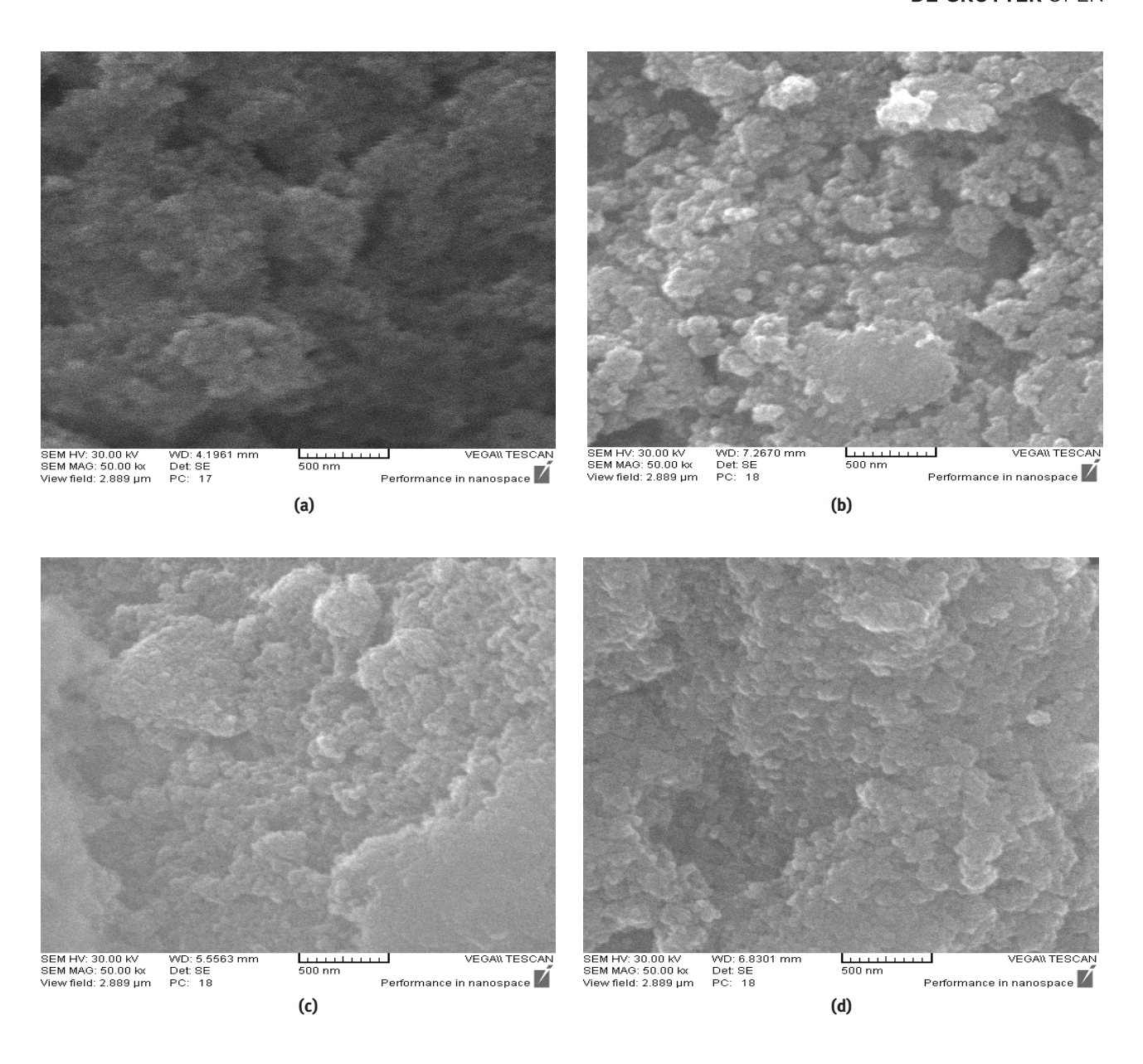


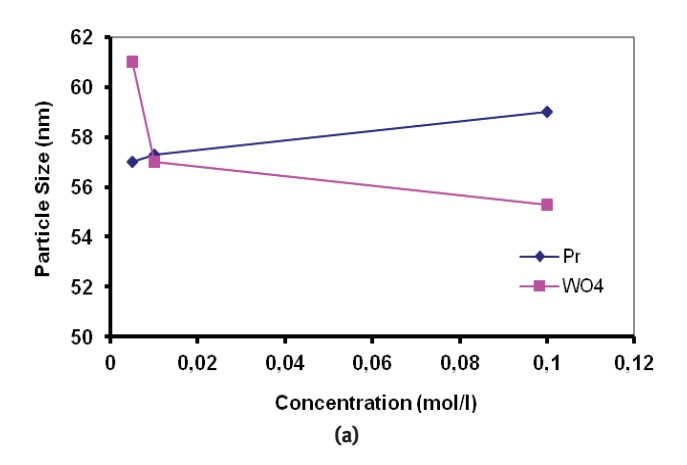
Figure 1: SEM images of $Pr_2(WO_4)_3$ nanoparticles synthesized via the chemical precipitation reaction at different runs of Table 1: (a) run 1, (b) run 3, (c) run 5, and (d) run 7.

the operating factors, the average value of the product diameters measured under each level was computed through the Taguchi routine [32,33], and these values were used to understand the pattern at which the product dimensions change upon varying the factors between the different levels, and the outcome was validated by the information conveyed in Figure 2. The images in Figure 2a show the effects of altering Pr^{3+} and $WO_4^{\ 2-}$ concentrations between the three different levels of 0.005, 0.01, and 0.1 mol/L on the size of the $Pr_2(WO_4)_3$. The image in Figure 2a suggests concentrations of 0.005 M and 0.1 M as being the optimum values for Pr^{3+} and $WO_4^{\ 2-}$ for yielding sample particles of the smallest size. Further, the image in Figure

2b, demonstrates the average effect of F_z values of 2.5, 10, and 40 ml/min, as well as temperature, on the product size. Based on the results one can conclude 10 mL/min as being the optimal F_z value. Additionally, one can see that 60° C is also an optimum temperature for the reaction and leads to the finest $Pr_z(WO_4)_3$ particles

Analysis of variance was carried out on the average particle dimensions of the samples produced according to Table 1 and the results are given in Table 2. The results shown in Table 2 show that What is seen is that at confidence interval of 90%, ignoring the interactions between the different parameters, all evaluated conditions, except F_2 , have considerable influences on the outcome of the reaction.

Considering the data presented in Figure 2 and the results of analysis of variance that are expressed in Table 2, the best direct precipitation reaction conditions are 0.005 mol/L for Pr^{3+} , 0.1 mol/L for WO_{λ}^{2-} and 60 °C.



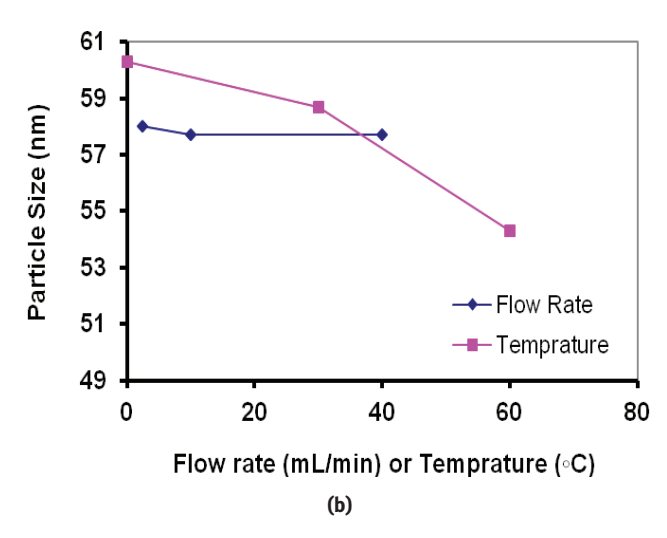


Figure 2: Average particle size of Pr₂(WO₄)₂ corresponding to the effect of each variable at various levels.

Based on the equation for evaluating the optimal outcome Y_{ont} (here the product size) proposed by the Taguchi design the following equation was used [28-33]:

$$Y_{opt} = \frac{T}{N} + (C_x - \frac{T}{N}) + (C_y - \frac{T}{N}) + (T_z - \frac{T}{N})$$
 (1)

Where, T/N is the average of all outcomes (here the average diameter of $Pr_2(WO_a)_3$) and C_x , C_y , and T_z are the average effect for the optimum conditions (here Pr3+ and WO,2concentrations and reaction temperature respectively). The optimum product diameter was calculated as 51 ± 1 nm, using equation and the optimum values. This value corresponds to the results of run 3 in Table 1 obtained from the analysis of variance experiments (i.e. 0.005 mol/L of Pr³⁺, 0.1 mol/L of WO_h²⁻ and 60 ${}^{\circ}$ C). The validity of this calculated value for the size was further confirmed by the SEM results (Figure 1b). Further TEM characterizations (Figure 3) not only confirmed this size by showing the experimental values to be around 50 nm, but also revealed the morphology of the product as spherical. Based on these evaluations, the product prepared under the conditions of run 3 was used for further analysis by energy dispersive X-ray analysis (EDX), XRD, FT-IR and UV-Vis.

3.1 Characterization of the optimal product

To evaluate the composition and purity of the optimum product its EDX and XRD patterns were acquired. Figure 4 shows the typical EDX pattern of synthesized Pr₂(WO₄)₂ nanoparticles. The EDX pattern showed that the product is highly pure, and the average atomic percentage ratio of Pr, W and O is about 8.3:27.4:64.3. This elemental analysis confirms the presence of the corresponding elements in stochiometric percentage. Also, its XRD pattern (Figure 5) shows strong intensities on a flat baseline, along with wide and low diffraction. The strong peaks observed in

Table 2: ANOVA results for the synthesis of Pr,(WO,), plates via precipitation procedure using OA, (34) matrix while the diameters of the synthesized Pr₂(WO₄)₃ plates (nm) are the responses.

		DOF			Pooled			
Factor	Code		S	٧	DOF	S'	F'	P'
Praseodymium concentration (mol/L)	Pr	2	6.9	3.45	2	6.9	30.9	5.8
Tungstate concentration (mol/L)	WO_4	2	50.9	25.45	2	50.9	228.1	43.8
Flow rate (ml/min)	F	2	0.2	0.1	-	-	-	-
Temperature (C)	T	2	57.6	28.8	2	57.6	258.0	49.6
Error	Ε	-	-	-	2	0.2	-	0.8

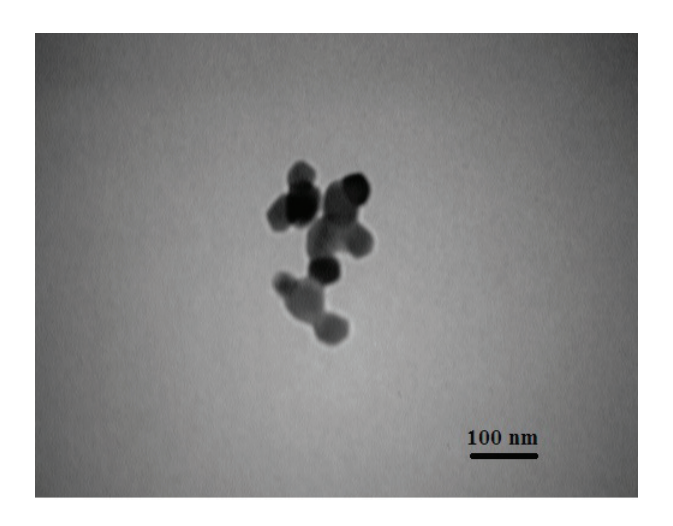


Figure 3: TEM image of $Pr_2(WO_4)_3$ nanoparticles synthesized by the precipitation reaction at optimum conditions.

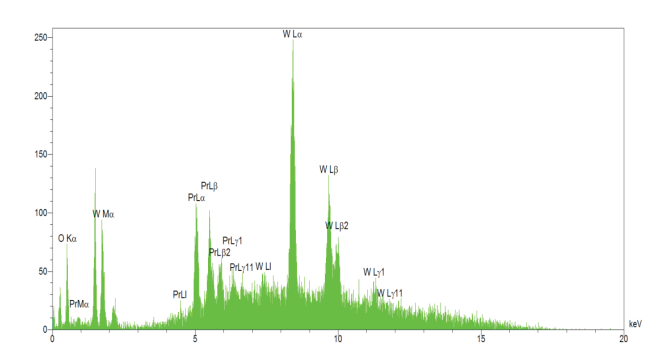


Figure 4: EDAX spectrum of synthesized $Sm_2(WO_4)_3$ nanoparticles by precipitation method.

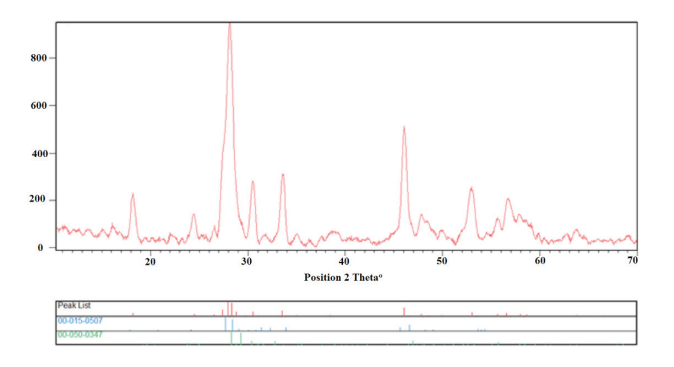


Figure 5: XRD pattern for synthesized $Pr_2(WO_4)_3$ nanoparticles by precipitation reaction at optimum conditions.

the spectrum are mainly in congruence with the pattern reported for the monoclinic and orthorhombic structures of $Pr_2(WO_4)_3$ according to PC-APD diffraction software codes (00-031-1153 and 00-050-0347).

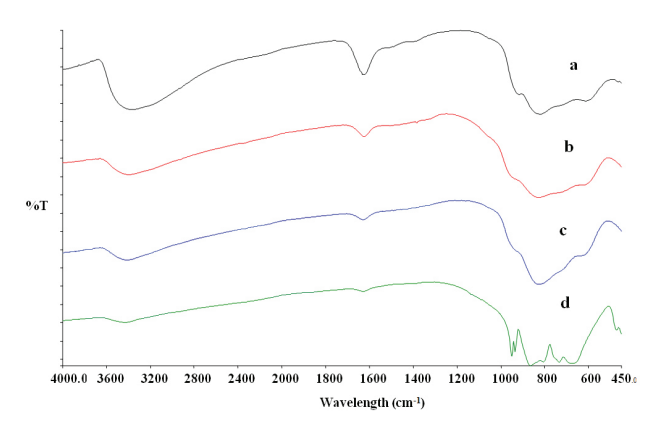


Figure 6: FT-IR spectra for $Pr_2(WO_4)_3$ nanoparticles prepared by the precipitation reaction at optimum conditions (a) before annealing, (b) after annealing at 200 °C, (c) after annealing at 450 °C, and (d) after annealing at 650 °C.

The FT-IR spectra of the sample were acquired both before and after annealing treatments at 200 °C, 450 ^oC and 650 ^oC and the results are given Figure 6. The absorption at 3370 cm⁻¹ in Figure 6a corresponds to the stretching and bending vibrations of the O-H bonds of the surface-absorbed water [3,4]. Naturally the annealing procedure leads to weakening and eventual elimination of this peak, while the absorption band of the monoclinic type structure appear between 473-881cm⁻¹ (Figure 6b-d), due to the annealing procedure. The IR spectra of the samples heated to 650 °C show split absorption peaks at 951, 937, 867, 810, 736, 680, 474 cm⁻¹ which correspond to monoclinic Pr₂(WO₄)₂, which suggests the transformation of the amorphous to crystalline phase which starts at 400 °C. This trend does not continue over 650 °C which indicates that the samples annealed up to this temperature have reached the maximum crystallinty [3,4].

The UV-Vis studies of the sample powder dispersed in an aqueous media were also performed and the results are given in Figure 7. The results show a main absorption peak at about 205 nm, indicating a small crystal size [1,28].

All of the experimental data acquired for the optimized method of the present work indicate that the products have good properties in terms of size, crystallinity and morphology, using a synthesis procedure that does not require costly and/or environmentally harmful reagents (e.g. templates, surfactants, or catalysts) that are common in the techniques used for the preparation of nanostructured materials.

Figure 8a shows the result of the UV-Vis diffuse reflectance spectroscopy (DRS) of the praseodymium tungstate nanoparticles. The optical band gap energy of the praseodymium tungstate nanoparticles can be measured

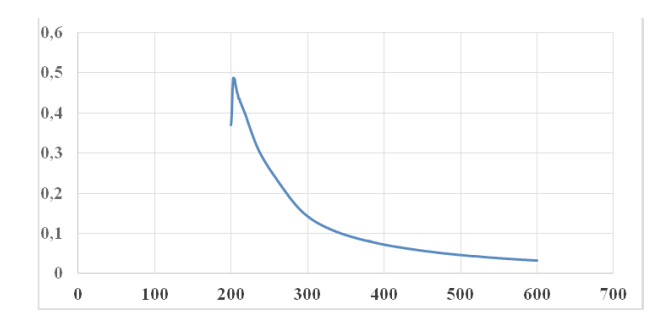
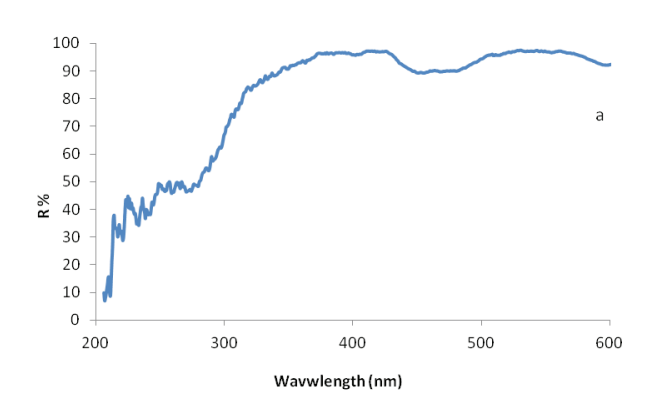


Figure 7: UV-Vis absorption spectra of the a Pr₂(WO₂) nano-particles (prepared under optimum conditions) dispersed in distilled water.



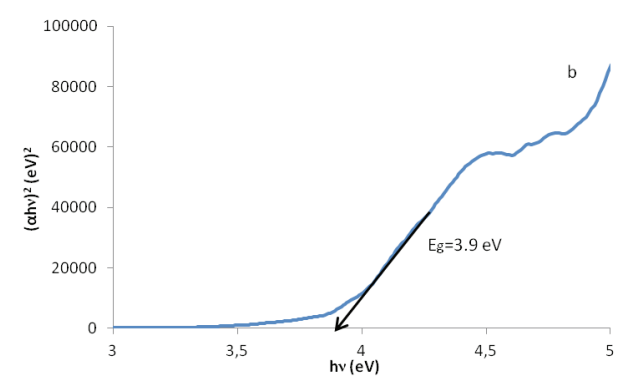


Figure 8: (a) UV-Vis diffuse reflectance spectra of as-synthesized praseodymium tungstate nanoparticles. (b) Tauc's plot for asprepared praseodymium tungstate nanoparticles.

using the diffuse reflectance data, while this parameter might be definitude as the required minimum photon energy for exciting an electron from the valence band of a semiconductor to the conduct band. Tauc's equation [34] can be utilized to determine the energy dependence of the semiconductors absorption edge:

$$\alpha h \nu = A(h \nu - E_{g})^{\eta} \tag{2}$$

Where α , h, ν , E_{σ}, A is the absorption coefficient, Planck's constant, frequency of light, band gap energy and proportional constant respectively. η may be equal to $\frac{1}{2}$

or 2 for the direct and indirect transitions respectively. In the present study η was equal to $\frac{1}{2}$ for the praseodymium tungstate nanoparticles. Figure 8b presents the Tauc's plot for the praseodymium tungstate nanoparticles. The estimated band gap for the sample is about 3.9 eV which corresponds to an absorption edge of about 318 nm.

3.2 Photocatalytic activity of nanomaterial

The photocatalytic activity of the praseodymium tungstate nanoparticles prepared under optimal conditions was investigated by following the photodegradation of methylene blue (MB) as a water contaminant under UV light illumination. MB in the presence of a photocatalyst commonly degrades to carbon dioxide, nitrate, ammonium and sulphate via the following reaction [35,36]:

$$MB + Pr_2(WO_4)_3 \text{ or } TiO_2 \rightarrow CO_2 + H_2O + NO_3^- + NH_4^+ + SO_4^{-2}$$

The concentration of pollution is related to the light absorbance of the studied solution according to the Lambert-Beer law as shown in equation 3 [37]:

$$A = \varepsilon bC$$
 (3)

Where C, A, ε , and b are the concentration of MB in the solution, light absorbance, the molar absorptivity and the path length of the light beam through the sample respectively. The Langmuir-Hinshelwood kinetics model was utilized to study the photocatalytic degradation kinetics of MB. This model is commonly used for the photocatalytic degradation of organic compounds when the initial concentration is low. This kinetic model is described by the following equation [37]:

$$-\frac{dC}{dt} = k_{app}C\tag{4}$$

Where k, t, C, and $-\frac{dC}{dt}$ are the reaction rate constant, the time of degradation, the concentration of MB and the rate of reaction respectively.

The values of MB concentration during irradiation at various time intervals (0, 10, 20, 30, 40, 50, and 60 minutes) monitored by UV-Vis absorbance are shown in Figure 9. In addition, Degussa P25 TiO₂, a well-known photocatalyst, was under the same conditions used to compare the photocatalytic activity of as-synthesized nanoparticles. Figure 10 shows the result of this comparison and represents the degradation of MB as a plot of C/Co and percentage of degradation versus illumination time, where C and C_o are the MB absorption at each irradiated time

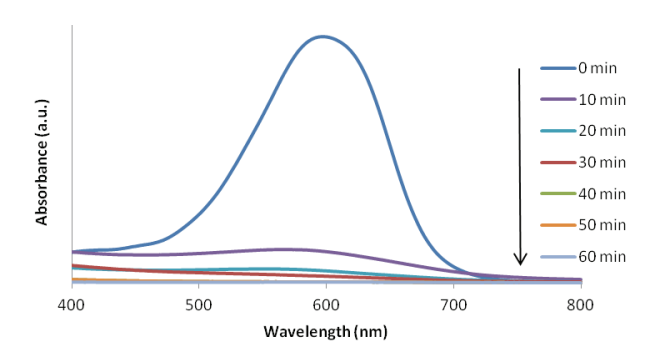


Figure 9: UV-Vis absorbance spectrum of MB at different time intervals on irradiation using 0.1 g/L praseodymium tungstate as photocatalyst (Temperature of the reactor was kept constant at 25±5 °C).

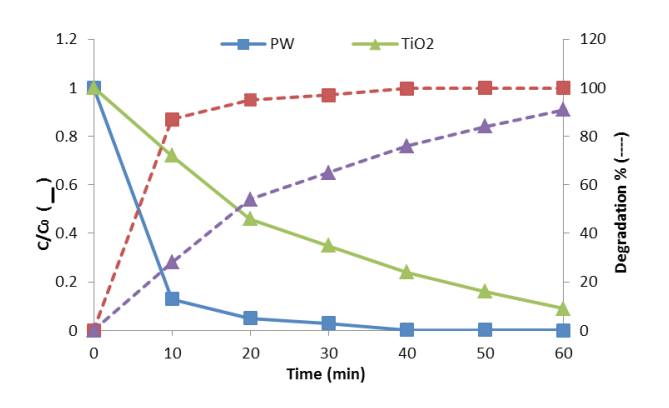


Figure 10: Comparison of photocatalytic degradation of MB solution under UV irradiation using praseodymium tungstate (PW) and Degussa P25 TiO₃ as photocatalysts.

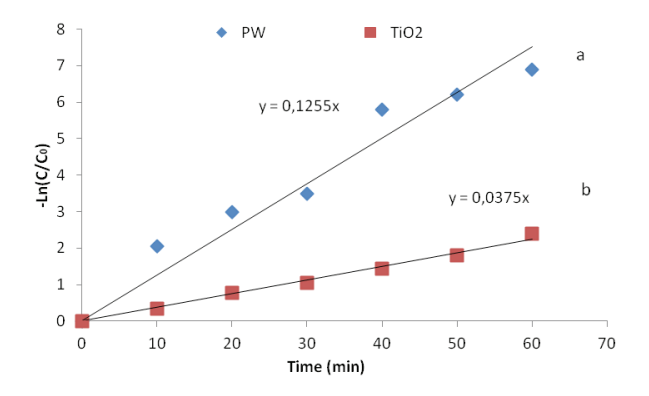


Figure 11: Pseudo first order kinetic of MB degradation for: a) praseodymium tungstate (PW), b) TiO₃.

and at time equals zero respectively. As shown in Figure 10, the maximum conversions of MB for praseodymium tungstate and TiO₂ respectively are about 99.7% and 76% after 40 minutes and about 99.9% and 91% 60 minutes after illumination. Figure 11 gives plot of MB degradation

as a pseudo first order reaction by using praseodymium tungstate nanoparticles. Thus, the first-order reaction rate constant was obtained as the slope of the linear regression of -ln(C/C_o) versus irradiation time. The results showed that the rate constants are 0.1255 and 0.0375 min⁻¹ for praseodymium tungstate and TiO₂ respectively. This means that praseodymium tungstate nanoparticles eliminate MB considerably quicker than TiO₂. These results are in agreement with previous reports [38-40] which explained that the main issue with the photocatalytic activity of TiO, is the recombination of electrons and holes. This substantially reduces the number of free charges on the surface and leads to a lower photocatalytic activity. Furthermore, the low adsorption ability of TiO₂ particles along with low quantum efficiency are other problems affecting the photocatalytic performance of TiO₂. However, the lattice of lanthanide compounds, e.g. praseodymium tungstate could provide better adsorption of an organic pollutant on the surface of semiconductor, causing higher photoactivity than TiO2. Furthermore, the special electronic structure of the lanthanide compounds leads to the different optical and photocatalytic performance than TiO₂ [40-42]. In conclusion, the results demonstrate that the praseodymium tungstate nanoparticles are a likely, beneficial and effective photocatalyst for organic pollutions purification from water.

4 Conclusion

The preparation of nanosized Pr₂(WO₂)₃ nanocrystals through a Taguchi-optimized precipitation reaction was evaluated. The optimization of the parameters at different levels suggested by the experimental design method showed that this simple precipitation route can be effectively used for the synthesis of praseodymium tungstate yielding products of good purity and dimensions. The ANOVA of the results indicated the concentrations of Pr³⁺ and WO_a²⁻ and the reactor temperature had the largest effect on the product properties. Different characterization techniques were used for the evaluation of the product and all revealed the effectiveness of the optimized method, and the comparison between the predictions and experimental results. Meanwhile, praseodymium tungstate has a better photocatalytic activity compared to TiO₂. In the presence of as-prepared praseodymium tungstate nanoparticles as photocatalyst, MB degradation yield was about 99.9% after 60 minutes of UV light irradiation, while TiO, degrades 91% of MB at the same time.

Acknowledgement: The financial support of this work by Iran National Science Foundation (INSF) and University of Tehran is gratefully acknowledged.

References

- [1] Rahimi-Nasrabadi M., S.M. Pourmortazavi, A.A. Davoudi-Dehaghani, S.S. Hajimirsadeghi, M.M. Zahedi, Synthesis and characterization of copper oxalate and copper oxide nanoparticles by statistically optimized controlled precipitation and calcination of precursor, CrystEngComm., 2013, 15, 4077-4086.
- [2] Pourmortazavi S.M., M. Taghdiri, N. Samimi, M. Rahimi-Nasrabadi, Eggshell bioactive membrane assisted synthesis of barium tungstate nanoparticles, Mater. Lett. 2014, 121, 5-7.
- Rahimi-Nasrabadi M., S.M. Pourmortazavi, M.R. Ganjali, S.S. Hajimirsadeghi, M.M. Zahedi, Electrosynthesis and characterization of zinc tungstate nanoparticles, J. Mol. Struct., 2013, 1047, 31-36.
- [4] Rahimi-Nasrabadi M., S.M. Pourmortazavi, M.R. Ganjali, A.R. Banan, F. Ahmadi, Synthesis procedure optimization and characterization of europium (III) tungstate nanoparticles, J. Mol. Struct., 2014, 1074, 85-91.
- [5] Lei F., B. Yan, Surfactant-assisted hydrothermal process, shape-control, and photoluminescence of Eu3+-doped lutetium tungstate microspheres, J. Mater. Res., 2011, 26, 88-95.
- [6] Tang Z., L. Zhou, F. Wang, L. Zhou, Synthesis, characterization and luminescence study of Eu(III) tungstates and molybdates nanotubes using carbon nanotubes as templates, Spectrochim. Acta, Part A, 2009, 72, 348-355.
- Grobelna B., P. Bojarski, B. Kuklinski, A. A. Kubicki, A. Synak, Optical properties and luminescence kinetics of Ln, Pr, (WO,) (where Ln = Gd, La) immobilized in silica xerogel, Opt. Mater., 2011, 34, 103-108.
- [8] Ronda C.R., T. Justel, H. Nikol, Rare earth phosphors: fundamentals and applications, J. Alloys Compd., 1998, 275-277, 669-676.
- [9] Venkateswarlu C., G.N. Hermantha Kumar, M. Seshadri, Y.C. Ratnakarm, K.S.R. Koteswarda Rao, J.L. Rao, Studies on optical absorption and photoluminescence properties of Pr3+ and Nd3+ doped mixed alkali chloroborate glasses, J. Alloys Compd., 2010, 502, 97-106.
- [10] Mahlik S., B. Kuklinski, M. Grinberg, L. Kostyk, O. Tsetkova, Acta Phys. Polon. A, Luminescence and Luminescence Kinetics of Gd₃Ga₂O₁₃ Polycrystals Doped with Cr³⁺ and Pr³⁺, Acta Phys. Pol., A, 2009, 117, 117-121.
- [11] Brown E., U. Hömmerich, T. Yamada, H. Yamane, J.M. Zavada, Spectroscopic characterization of praseodymium doped gallium nitride powder prepared by a Na flux method, J. Alloys Compd., 2009, 488, 628-631.
- [12] Grobelna B., P. Bojarski, The effect of WO, 2- group in xerogels doped with $Ln_{2,\nu}Pr_{\nu}(WO_{\nu})_3$ where Ln = La, Gd, Opt. Appl., 2010, 40, 359-366.
- [13] Chen J., X. Gong, Y. Lin, Y. Chen, Z. Luo, Y. Huang, Synthesis and spectral property of Pr3+-doped tungstate deep red phosphors, J. Alloys Compd., 2010, 492, 667-670.

- [14] Yang X., X. Yu, H. Yang, Y. Guo, The investigation of optical properties by doping halogen in the BaMoO,:Pr3+ phosphor system, J. Alloys Compd., 2009, 479, 307-309.
- [15] Guo W., Y. Lin, X. Gong, Y. Chen, Z. Luo, Y. Huang, Polarized spectral properties of Pr3+ ions in NaGd(MO,), crystal, Appl. Phys. B, 2009, 94, 155-164.
- [16] Tian L., S.-I. Mho, Enhanced luminescence of SrTiO₂:Pr³⁺ by incorporation of Li+ ion, Solid State Commun., 2003, 125,
- [17] Amano F., E. Ishinaga, A. Yamakata, Effect of particle size on the photocatalytic activity of WO₂ particles for water oxidation, J. Phys. Chem. C, 2013, 117, 22584-22590.
- [18] Bouslama M., M. C. Amamra, Z. Jia, M. Ben Amar, K. Chhor, O. Brinza, et al, Nanoparticulate TiO₃-Al₃O₃ photocatalytic media: effect of particle size and polymorphism on photocatalytic activity, ACS Catal., 2012, 2, 1884-1892.
- [19] Kaczmarek S.M., E. Tomaszewicz, D. Moszynski, A. Jasik, G. Leniec, DTA/TG, IR, EPR and XPS studies of some praseodymium(III) tungstates, Mater. Chem. Phys., 2010, 124, 646-651.
- [20] Yoshimura M., H. Morikawa, M. Miyake, Preparation and cell parameters of new rare-earth tungstates $R_{10}W_{22}O_{81}$ (R = La, Ce, Pr and Nd), Mater. Res. Bull., 1975, 10, 1221-1224.
- [21] Nassau K., H.J. Levinstein, J.M. Loiacini, A comprehensive study of trivalent tungstates and molybdates of the type L₂(MO₄)₃, J. Phys. Chem. Solids, 1965, 26, 1805-1816.
- [22] Brixner L.N., A.W. Sleight, Crystal growth and precision lattice constants of some Ln₂(WO₄)₂-type rare earth tungstates, Mater. Res. Bull., 1973, 8, 1269-1273.
- [23] Pourmortazavi S.M., S.S. Hajimirsadeghi, M. Rahimi-Nasrabadi, Statistical optimization of condition for synthesis lead sulfide Nanoparticles, Mater. Manuf. Processes, 2009, 24, 524-528.
- [24] Pourmortazavi S.M., M. Rahimi-Nasrabadi, A.A. Davoudi-Dehaghani, A. Javidan, M.M. Zahedi, S.S. Hajimirsadeghi, Statistical optimization of experimental parameters for synthesis of manganese carbonate and manganese oxide nanoparticles, Mater. Res. Bull., 2012, 47, 1045-1050.
- [25] Pourmortazavi S.M., M. Rahimi-Nasrabadi, S. S. Hajimirsadeghi and I. Kohsari, Optimization of Parameters for the Synthesis of Silver Iodate Submicron Belts by Taguchi Robust Design Method, Chem. Eng. Commun., 198 (2011) 1182-1188.
- [26] Bayat Y., S. M. Pourmortazavi, H. Ahadi, H. Iravani, Taguchi robust design to optimize supercritical carbon dioxide antisolvent process for preparation of 2,4,6,8,10,12-hexanitro-2-,4,6,8,-10,12-hexaazaisowurtzitane nanoparticles, Chem. Eng. J., 2013, 230, 432-438.
- [27] Rahimi-Nasrabadi M., M.B. Gholivand, A.R. Vatanara, H. Batooli, Comparison of essential oil composition of Eucalyptus oleosa obtained by supercritical carbon dioxide and hydrodistillation, J. Herbs Spices Med. Plants, 2012, 18, 318-330.
- [28] Pourmortazavi S.M., M. Rahimi-Nasrabadi, M. Khalilian-Shalamzari, M.M. Zahedi, S.S. Hajimirsadeghi, I. Omrani, Synthesis, structure characterization and catalytic activity of nickel tungstate nanoparticles, Appl. Surf. Sci., 2012, 263, 745-752.
- [29] Pourmortazavi S.M., M. Rahimi-Nasrabadi, S. S. Hajimirsadeghi, Applying the Taguchi robust design to optimization of the experimental conditions for synthesis of lead chromate nanorods, J. Dispersion Sci. Technol., 2012, 33, 254-257.

- [30] Pourmortazavi S.M., S. S. Hajimirsadeghi, M. Rahimi-Nasrabadi, M.M. Zahedi, Taguchi robust design to optimize synthesis of lead oxalate nano-disks, Mater. Sci. Semicond. Process., 2013, 16, 131-137.
- [31] Pourmortazavi S.M., S.S. Hajimirsadeghi, M. Rahimi-Nasrabadi, I. Kohsari, Electrosynthesis and characterization of copper oxalate nanoparticles, Synth. React. Inorg. Met.-Org. Chem., 2012, 42, 746-751.
- [32] Rahimi-Nasrabadi M., S.M. Pourmortazavi, M. Khalilian-Shalamzari, S.S. Hajimirsadeghi, M.M. Zahedi, Optimization of synthesis procedure and structure characterization of manganese tungstate nanoplates, Cent. Eur. J. Chem., 2013, 11, 1393-1401.
- [33] Pourmortazavi S.M., M. Rahimi-Nasrabadi, M. Khalilian-Shalamzari, H. R. Ghaeni, S.S. Haiimirsadeghi, Facile chemical synthesis and characterization of copper tungstate nanoparticles, J. Inorg. Organomet. Polym., 2014, 24, 333-339.
- [34] Tauc J., R. Grigorovici, A. Vancu, Optical properties and electronic structures of amorphous germanium, Phys. Status Solidi, 1966, 15, 627-637.
- [35] Parida K.M., N. Sahu, Visible light induced photocatalytic activity of rare earth titania nanocomposites, J. Mol. Catal. A: Chem., 2008, 287, 151-158.
- [36] Stengl V., S. Bakardjieva, N. Murafa, Preparation and photocatalytic activity of rare earth doped TiO, nanoparticles, Mater. Chem. Phys., 2009, 114, 217-226.

- [37] Natarajan T.S., K. Natarajan, H.C. Bajaj, R.J. Tayade, Energy efficient UV-LED source and TiO, nanotube array-based reactor for photocatalytic application, Ind. Eng. Chem. Res., 2011, 50, 7753-7762.
- [38] Reszczynska J., D. Arenas Esteban, M. Gazda, A. Zaleska, Pr-doped TiO2. The effect of metal content on photocatalytic activity, Physicochem. Probl. Miner. Process., 2014, 50, 515-524.
- [39] Ghasemi S., S. Rahman Setayesh, A. Habibi-Yangjeh, M. R. Hormozi-Nezhad, M. R. Gholami, Assembly of CeO₂-TiO₂ nanoparticles prepared in room temperature ionic liquid on graphene nanosheets for photocatalytic degradation of pollutants, J. Hazard. Mater., 2012, 199-200, 170-178.
- [40] Farbod M., M. Kajbafvala, Effect of nanoparticle surface modification on the adsorption-enhanced photocatalysis of Gd/TiO₂ nanocomposite, Powder Technol., 2013, 239, 434-440.
- [41] Maeda K., K. Domen, Photocatalytic water splitting: recent progress and future challenges, J. Phys. Chem. Lett., 2010, 1, 2655-2661.
- [42] Sohrabi S., F. Akhlaghian, Light expanded clay aggregate (LECA) as a support for TiO2, Fe/TiO2, and Cu/TiO2 nanocrystalline photocatalysts: a comparative study on the structure, morphology, and activity, J. Iran Chem. Soc., 13, 2016, 1785-1796.